$CuMn_2O_4$: properties and the high-pressure induced Jahn-Teller phase transition

2001 J. Phys.: Condens. Matter 13 2549

(http://iopscience.iop.org/0953-8984/13/11/311)

INSTITUTE OF PHYSICS PUBLISHING JOURNAL OF PHYSICS: CONDENSED MATTER

J. Phys.: Condens. Matter **13** (2001) 2549–2562 www.iop.org/Journals/cm PII: S0953-8984(01)17657-5

$CuMn_2O_4$: properties and the high-pressure induced Jahn–Teller phase transition

A Waśkowska[1], L Gerward[2], J Staun Olsen[3], S Steenstrup[3] and E Talik[4]

[1] Institute of Low Temperature and Structure Research, Polish Academy of Sciences, 50 950 Wrocław, Poland
[2] Department of Physics, Technical University of Denmark, 2800 Kongens Lyngby, Denmark
[3] N Bohr Institute, Ørsted Laboratory, University of Copenhagen, 2100 Copenhagen, Denmark
[4] Institute of Physics, Silesian University in Katowice, 40 007 Katowice, Poland

Received 3 October 2000, in final form 25 January 2001

Abstract

Single crystal x-ray diffraction, x-ray photoelectron spectroscopy and magnetic susceptibility measurements at normal pressure have shown that, in spite of two Jahn–Teller active ions in $CuMn_2O_4$, the crystal is cubic with partly inverse spinel structure, the inversion parameter being $x = 0.8$. The cation configuration at normal pressure was determined as $Cu^{+}_{0.2}Mn^{2+}_{0.8}[Cu^{2+}_{0.8}Mn^{3+}_{0.2}Mn^{4+}_{1.0}]O_4$. The high-pressure behaviour of the crystal was investigated up to 30 GPa using the energy dispersive x-ray diffraction technique and synchrotron radiation. A first-order phase transition connected with a tetragonal distortion takes place at $P_c = 12.5$ GPa, the c/a ratio being 0.94 at $P = 30$ GPa. The high-pressure phase has been described in terms of ligand field theory and explained by the changes to the valence and electronic configuration of the metal ions, leading to the formula $Cu^{2+}_{0.2}Mn^{3+}_{0.8}[Cu^{2+}_{0.8}Mn^{3+}_{1.2}]O_4$. The electron configuration of the tetrahedrally coordinated Cu^{2+} and Mn^{3+} is $(e^4)t^5$ and e^2t^2, respectively. On the other hand, the electron configuration of Cu^{2+} located at octahedral sites is $(t^6_{2g})e^3_g$. While six electrons with antiparallely aligned spins occupy the triplet (t^6_{2g}), three electrons on the orbital e_g can be distributed in two ways (double degeneracy): $(d_{x^2-y^2})^1(d_{z^2})^2$ and $(d_{x^2-y^2})^2(d_{z^2})^1$. The first alternative leads to an axially elongated octahedron; the second one causes flattening of the octahedron. The contraction of the c axis indicates, that in the high-pressure phase the second configuration with unpaired electron on the d_{z^2} orbital occurs. A similar effect of the octahedral contraction brings the orbital degeneracy of Mn^{3+} with the $t^3_{2g}e^1_g$ distribution. It follows that at high pressure the ligand field forces the two metals to take the valences that they show in the parent oxides CuO and Mn_2O_3.

1. Introduction

There is a revival of interest in compounds containing copper and manganese oxides with perovskite and spinel structures, stimulated by the effect of mixed valence states of the two transition metals with 3d electronic configuration in heavy fermion systems and high T_c superconductors. Lithium manganospinels have industrial interest due to their potential use as cathode material of rechargeable batteries.

Binary manganese oxides with the spinel structure ($M^{II}Mn_2O_4$, M = Ni, Cu, Zn, Ga) are interesting because of their pressure and temperature dependent structural instability and the related change of the electronic configuration of the Mn cations involved in superexchange magnetic interactions [1] and electronic transport phenomena [2–4]. In the present paper we will concentrate on the high-pressure phase transition in $CuMn_2O_4$ and relate it to the Jahn–Teller (JT) activity of $Cu^{2+}(d^9)$ and $Mn^{3+}(d^4)$ cations.

There exists already a vast literature describing various properties of this spinel. Nevertheless, the conclusions are still inconsistent. For instance, based on x-ray diffraction [5–10] and neutron diffraction studies [2, 11, 12], $CuMn_2O_4$ was reported to be an inverted cubic spinel with lattice constant $a = 8.327(2)$ Å, space group $Fd\bar{3}m$ and the formula $Cu_{1-x}Mn_x[Cu_xMn_{2-x}]O_4$, where [ ] denotes octahedral sites. The observed inversion parameter x ranges from $x = 0$ (normal cation distribution) to $x = 1$ (completely inverted spinel). The ionic states of the copper and manganese cations are not evident because the two cations located either at tetrahedral (A) or octahedral [B] sites should produce a JT distortion of the cubic crystal.

To explain the cubic symmetry, a model with two opposite effects has been proposed: a distortion corresponding to $c/a > 1$ at the B sites and another compensating distortion ($c/a < 1$) at the A sites [6, 7, 13, 14]. It is however, unlikely that only Mn^{3+} or Cu^{2+} should be present, because the high electric conductivity in $CuMn_2O_4$ [3, 15] requires that the same metal ions should be present in mixed valence states enabling electron hopping at either the tetrahedral or the octahedral sites. Therefore, various possible valence assignments have been proposed: $Cu^+[Mn^{3+}_{2-x}Mn^{4+}_x]O_4$, $Cu^{2+}[Mn^{2+}_{2-x}Mn^{4+}_x]O_4$, $Cu^{2+}_{1-x}Cu^+_x[Mn^{3+}_{2-x}Mn^{4+}_x]O_4$ and other combinations with partly inverted distributions. These formulae suggest another explanation of the cubic symmetry, namely that the amount of the distortive ions at each site is insufficient to cause any observable distortion [14]. The critical fraction of distortive ions should be about 55%. At high temperature the anomalous phase transition has been observed by thermal difference analysis (DTA) and a rapid increase of electrical resistivity above $T_k \sim 750$ K. Some authors [14, 15] have concluded that the ionic configuration changes from $Cu^+[Mn^{3+}Mn^{4+}]O_4$ at room temperature, to the tetragonal $Cu^{2+}[Mn^{3+}]_2O_4$ above T_k but no diffraction data on this phase have been reported.

It follows from the above that experimental data, including x-ray absorption edge measurements [16] and photoelectron spectroscopy (XPS) [17, 18], indicate that, at ambient conditions, the cubic copper manganese oxide exists in a broad range of ionic configurations of the spinel structure.

The aim of the present work is to show the effect of high pressure (HP) on the crystal structure stability and the JT-distorting properties of the 3d metal ions. The five d orbitals in the octahedral ligand field are split into a lower triplet t_{2g} and an upper doublet e_g. The electronic configuration of the d^4 orbital of Mn^{3+} is $t^3_{2g}e^1_g$ and the configuration of the d^9 orbital of Cu^{2+} is $(t^6_{2g})(e^2_g)e^1_g$, where configurations in parentheses denote paired electron spins. When these ions are subjected to the tetrahedral ligand field, their configurations are given as $e^2t^2_2$ and $(e^4)(t^4_2)(t^1_2)$ for Mn^{3+} and Cu^{2+}, respectively [19, 20]. Orbitally degenerate electron configurations of d states with unpaired spins are unstable in the ligand field. Therefore, we

expect that applying pressure will change the electronic states of Cu and Mn ions in such a way that the degeneracy of the orbitals increases. At some point, this should result in a structural phase transition.

Our recent studies on $NiMn_2O_4$ [21, 22], $CuGaMnO_4$ [23] and $ZnMn_2O_4$ [24] have shown a temperature and pressure dependent polymorphism, related to electronic configurations of the 3d cations. In light of the ambiguities mentioned above, concerning the configuration of the valence electrons in $CuMn_2O_4$, our first efforts have been directed to an adequate characterization of the starting material. We have redetermined the single crystal structure at ambient conditions, as structural parameters are important for the further study. We have also examined the cation valences by x-ray photoelectron spectroscopy (XPS) and confirmed it by magnetic susceptibility measurements. Finally, high-pressure x-ray diffraction was applied to study the expected phase transition.

2. Experiment

Samples of $CuMn_2O_4$ were prepared by prolonged heating of an equimolar mixture of CuO and Mn_2O_3 in an evacuated silica tube at 1323 K. After 12 days the samples were brought to room temperature with a cooling rate of about 6 K/hour [8].

The single crystal structure redetermination at normal conditions was done with a KM-4 diffractometer (Kuma Diffraction). A least-squares fit of the unit cell dimensions without symmetry constraints showed the crystal to be cubic. Crystal data and a summary of the experimental conditions for the intensity data collection and structure refinement are given in table 1. In the structure calculation by full matrix least squares, a model with normal cation distribution converged to $R = 0.051$ (R is the crystallographic discrepancy factor). Another approach with a partly inverted spinel was started with the Cu and Mn ions located simultaneously at tetrahedral and octahedral positions in proportion 0.5:0.5. Their site occupation parameters, varied under constraints of 8(a) and 16(d) site symmetry, were refined and led to $R = 0.024$. On the basis of the lower R-value we propose the latter model with the parameters given in table 2. The origin of the unit cell was taken at the point $\bar{3}m$ of space group $Fd\bar{3}m$. All calculations were performed with the SHELXL'93 program system [25].

The XPS spectra were obtained with monochromatized Al Kα radiation using a PHI 5700/660 Physical Electronics spectrometer. The photoelectron spectra were analysed by a hemispherical mirror analyser with an energy resolution of about 0.3 eV. To obtain a fresh surface, the samples were broken in 10^{-10} Torr vacuum. The carbon C 1s peak with binding energy of 284.5 eV was used for calibration.

Magnetic susceptibility was measured using the Faraday method with magnetic fields 250–1000 Oe and temperatures 4.2–700 K in helium atmosphere.

High pressure powder-diffraction spectra were recorded using synchrotron radiation and the white-beam energy dispersive method. The experiments were performed at the Hamburg Synchrotron Radiation Laboratory (HASYLAB), Germany. High pressures in the range 0–30 GPa were obtained in a Syassen–Holzapfel-type diamond-anvil cell. The sample and the ruby chip were contained in a hole of diameter 0.2 mm in an Inconel gasket. A 4:1 methanol:ethanol mixture was used as the pressure transmitting medium. The pressure was determined by measuring the wavelength shift of the ruby red line and applying the nonlinear pressure scale of Mao *et al* [26]. The Bragg angle was calculated from a zero pressure diffraction spectrum of NaCl in the diamond-anvil cell. The standard deviation of the pressure determination (e.s.d.) was about 0.1 GPa for pressures below 10 GPa. For higher pressure the e.s.d. may be larger because of quasi-hydrostatic conditions.

Table 1. Details of single crystal x-ray data collection and structure refinement at ambient pressure.

Crystal data	
Crystal system	Cubic
Space group	$Fd\bar{3}m$
a (Å)	8.334(1)
V (Å^3)	578.84(3)
Z	8
Density calc. (Mg m^{-3})	5.449
Absorption coeff. μ (mm^{-1})	15.69
Data collection	
Radiation, wavelength (Å)	Mo Kα, 0.710 73
Monochromator	graphite
2θ range (°)	88.5
Scan type	$\omega/2\theta$
Scan width (°)	$1.1 + 0.25 \tan\theta$
Index range	h: -16, 16
	k: -16, 0
	l: 0, 16
No of reflections collected	2443
No of independent reflections	125
No of observed reflections	112
Decay of standard reflections	negligible
Refinement	
Refinement on	F^2
F_o criterion	$\lvert F_o\rvert \geqslant 4\sigma(F_o)$
Corrections:	
Lorentz—polarization	
Absorption (analytical), T_{min} and T_{max}	0.46 and 0.58
Extinction (empirical as in SHELXL93)	$x = 0.0032(1)$
R_{int} (before; after absorption)	0.094; 0.048
Number of varied parameters	10
Final R_1	0.024
Final wR_2	0.045
Goodness of fit	1.191
Min. and max. residual (e Å^{-3})	-1.8, 0.9

3. Results and discussion

From the single crystal structure calculations with refined site occupation parameters (SOPs in table 2) we conclude that the crystal is cubic ($Fd\bar{3}m$) with the following cation distribution:

$$(Cu_{0.2}Mn_{0.8})[Cu_{0.8}Mn_{1.2}]O_4. \quad (1)$$

We propose that the sample is a partly inverted spinel with inversion parameter $x = 0.8$. The observed cubic symmetry can be explained by taking into consideration a spin superexchange process via the common O^{2-} ion linking the A-site cation (M_A) to the B-site cation (M_B) in the spinel structure. A direct charge transfer at tetrahedral sites would be unlikely due to the long distance between the M_A ions (3.609 Å). As indicated in table 3, the nearest-neighbour distance for the A and B sites is 3.071 Å, and the angle Mn_A–O–Mn_B

Table 2. Atomic positonal parameters and thermal displacement amplitudes U_{iso} (Å^2), together with site occupation factors (SOFs) for a partly inverted spinel.

Atom	Site	x	y	z	U_{iso}	SOF
Cu/Mn	8(a)	1/8	1/8	1/8	0.0102(2)	0.21(5):0.78(7)
Cu/Mn	16(d)	1/2	1/2	1/2	0.0118(3)	0.80(8):1.17(11)
O	32(e)	0.2552(2)	0.2552(2)	0.2552(2)	0.0144(6)	1.0

Table 3. Selected interatomic distances and bond angles in the cubic $CuMn_2O_4$. M_A and M_B denote the Cu and Mn cations located on the A and B sites, respectively.

Distances (Å)			Angles (°)		
M_A–O	1.880(2)	(4×)	O–M_A–O	109.47(0)	(4×)
M_B–O	2.041(2)	(6×)	O–M_B–O	180.(0)	(3×)
M_A–M_A	3.609(0)		O–M_B–O	87.5(1)	(6×)
M_B–M_B	2.946(0)		O–M_B–O	92.4(1)	(6×)
M_A–M_B	3.071(0)		M_A–O–M_B	123.53(7)	

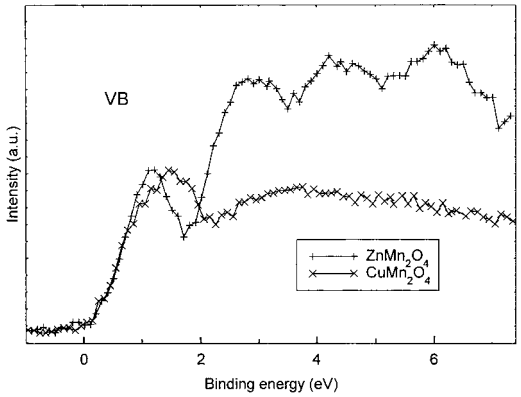

Figure 1. XPS valence band spectrum of $CuMn_2O_4$.

is 123.53(7)°. Such a configuration enables superexchange coupling which involves electron transfer: Mn_A^{3+}–O^{2-}–$Mn_B^{3+} \rightarrow Mn_A^{2+}$–$O^{-}$–$Mn_B^{4+}$. Thus, a possible valence configuration would be

$$Cu_{0.2}^{2+}Mn_{0.8}^{2+}[Cu_{0.8}^{2+}Mn_{1.2-0.8}^{3+}Mn_{0.8}^{4+}]O_4. \tag{2}$$

Also, the low value of the oxygen positional parameter in the crystal cell (0.2552(2), table 2) is an indication of the inverse spinel with a considerable fraction of Mn^{4+} (ionic radii are: $r_{Mn^{3+}} > r_{Mn^{4+}}$). The replacement of Mn^{3+} by the JT inactive Mn^{2+} and Mn^{4+} plays the key role in suppressing the tetragonal distortion (e.g. [27]). However, a preference of Cu^{2+} for the B sites cannot be ruled out. In order to correlate the electronic configuration of these ions with the observed cubic symmetry we refer to our XPS results.

Figure 1 shows the valence band (VB) spectrum, arising from a hybridization of the Mn 3d, Cu 3d and O 2p core levels. For comparison, the VB of $Zn^{2+}[Mn^{3+}]_2O_4$ with well defined ionic valences is also shown. The two spectra are similar in character at the Fermi level with the cut-off suggesting metallic behaviour of these compounds. The peak observed for $ZnMn_2O_4$ at the binding energy (BE) = 1.0 eV is also present in the $CuMn_2O_4$ spectrum, but the latter is broadened and shifted to 1.3 eV. Besides, the wide energy band above 2.5 eV, without any

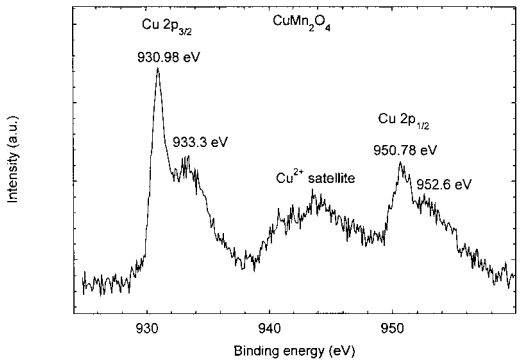

Figure 2. XPS spectra of Cu 2p core levels.

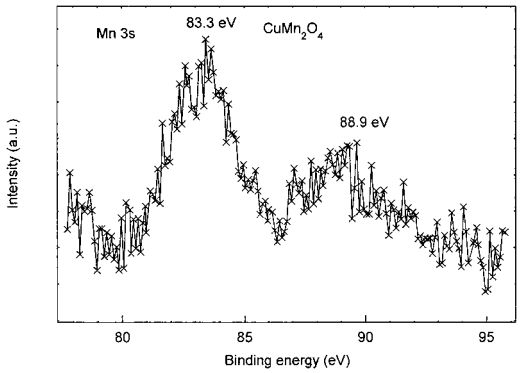

Figure 3. XPS spectrum of Mn 3s core level in $CuMn_2O_4$.

characteristic features corresponding to unequivalent ions, suggests that the photoemission final stages of the mixed valence ions are close in energy and strongly hybridized.

Figure 2 shows the binding energies of the Cu 2p core levels. The spectrum shows the spin–orbit components Cu $2p_{3/2}$ and Cu $2p_{1/2}$, at about 931 and 951 eV, respectively. Besides, a satellite peak at about 944 eV can be observed. The Cu $2p_{3/2}$ signal has a sharp peak at 931.0 eV and another peak at 933.3 eV, which is characteristic of Cu^{2+} having the d^9 configuration in the ground state. Brabers and van Setten [28] assigned a peak at 930.5 eV to Cu^+ on the A site and at 932.6 eV to Cu^{2+} on the B site in $CuCoMnO_4$. It has been shown that for Cu_2O, CuO and for high-temperature super-conductors this satellite occurs if Cu^+ and Cu^{2+} ions are present simultaneously [29–33].

The Mn 3s spectrum is split into two lines at 83.3 eV and 88.9 eV (figure 3) due to the exchange interactions between the s core hole and the 3d spins. This leads to an energy difference between the photoemission final states with the s electrons parallel or antiparallel to the 3d spin. The Mn s splitting is 5.6 eV in agreement with observations for Mn_2O_3 [34]. The Mn 3p asymmetric spectrum (figure 4) confirms the x-ray diffraction result regarding the mixed valence states of the Mn ions. Comparing the Mn 3p spectrum with those of reference compounds containing Mn^{2+} in Mn_2TiO_4, Mn^{3+} in $ZnMn_2O_4$ and Mn^{4+} in $MgNiMnO_4$ Töpfer *et al* [32] explained the broadening of the Mn 3p line and the BE values as a result of superposition of the signals from three, simultaneously present valence states of the Mn ion. However, the difference in binding energy between the lower and higher valences is about 1 eV,

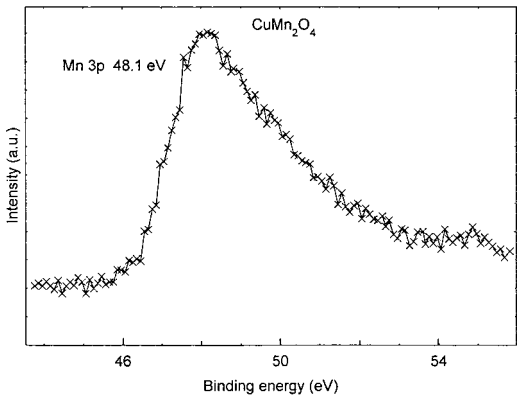

Figure 4. The Mn 3p spectrum of $CuMn_2O_4$.

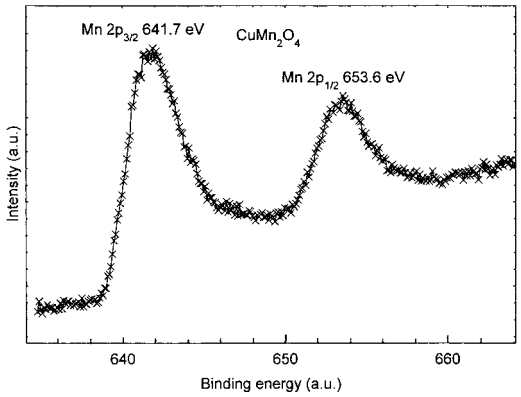

Figure 5. The Mn 2p core level.

which is smaller than the FWHM (full width at half maximum) of the signal [35], and therefore the primary and satellite peaks overlap. The Mn 2p core level has also been measured (figure 5). The spectrum displays the spin–orbit doublet of Mn $2p_{3/2}$ and Mn $2p_{1/2}$ located at 641.7 and 653.6 eV, respectively. The peaks are shifted by $\sim$1.7 eV towards a higher binding energy as compared with pure Mn metal (BE = 639 eV and 650 eV for $2p_{3/2}$ and $2p_{1/2}$, respectively). This shift suggests several valence states of Mn in this compound. However, the satellite peak accompanying the Mn $2p_{3/2}$ signal overlaps the main Mn $2p_{1/2}$ and cannot be resolved. Such a situation is observed also in other manganites [18, 32, 33, 35].

The shape of the O 1s signal is of some interest as well (figure 6). It is formed by two lines at 529.45 eV and 531.5 eV. The first binding energy corresponds to the one found for CuO (529.2 $\pm$ 0.2 eV), the second energy is 1.3 eV larger than the peak observed for Cu_2O (530.2 $\pm$ 0.2 eV) [36]. A similar O 1s spectrum consisting of two main structures at 528.9 and 532 eV has been reported for $YBa_2Cu_3O_{7-\delta}$ and the effect was attributed to surface degradation [37].

Summarizing the results of XPS measurements we conclude that also the Cu ions are present in two valence states, Cu^{2+} and Cu^{+}, in $CuMn_2O_4$. In agreement with a concept of the site preference, the Cu^{2+} ions occupy B sites and assuming the interaction

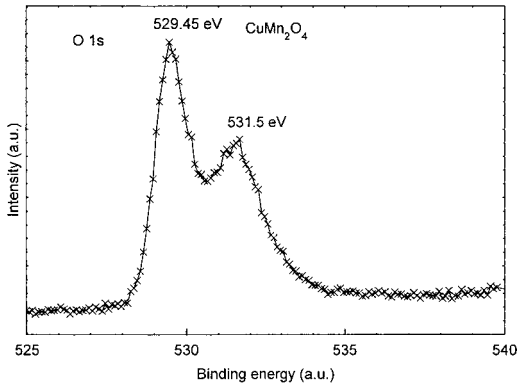

Figure 6. XPS O 1s signal in $CuMn_2O_4$.

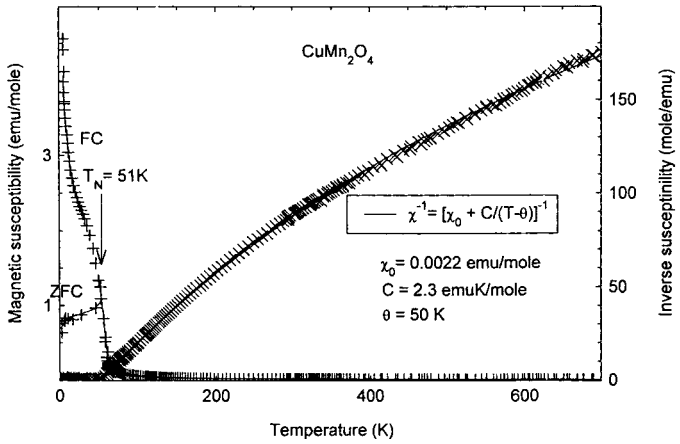

Figure 7. Temperature dependence of the magnetic susceptibility χ and χ^{-1}.

$Cu_A^{2+} + Mn_B^{3+} \rightarrow Cu_A^{+} + Mn_B^{4+}$, formula (2) should be modified accordingly:

$$Cu^{+}_{0.2}Mn^{2+}_{0.8}[Cu^{2+}_{0.8}Mn^{3+}_{(0.4-0.2)}Mn^{4+}_{1.0}]O_4. \tag{3}$$

At this concentration of Mn^{3+} on the B sites there should be no tetragonal distortion due to the Mn^{3+} ions alone. The observed cubic symmetry cannot be broken by the Cu^{2+} ions either, as their fraction at the B sites is less than the critical amount of about 55% mentioned in the introduction. Also Cu^{+} with a filled d^{10} shell is in a stable configuration.

The temperature dependence of the magnetic susceptibility, χ and its inverse χ^{-1} is shown in figure 7. The inverse magnetic susceptibility follows the Curie–Weiss behaviour above ∼400 K. Below 200 K, the convex deviation of the plot χ^{-1} against T can be ascribed to the crystal-field splitting of the d orbitals of the Cu and Mn ions. The temperature dependence of zero-field-cooling (ZFC) shows a maximum at $T_N = 51$ K, which is absent under FC (field-cooling) conditions. The difference in behaviour between ZFC and FC indicates that some small ferromagnetic ordering is forced on field cooling and it hinges on Cu^{2+}–Mn^{3+} and Cu^{+}–Mn^{4+} interactions, confirming the sample to be ferrimagnetic. The magnetic moment is $\mu = 1.53\mu_B$ based on ligand field effects and cation valences according to the x-ray and XPS measurements. This value is somewhat low compared to μ_{eff} resulting from the Curie constant and with the assumed formal valencies of Cu^{2+} and Mn^{3+}. Nevertheless, it can be

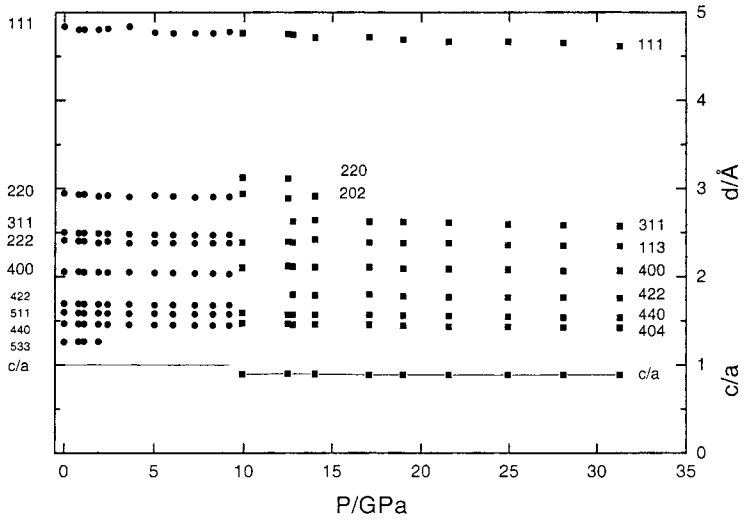

Figure 8. Observed lattice plane spacings, d_{hkl}, of $CuMn_2O_4$ as functions of pressure. Circles denote the cubic phase, and squares the tetragonal phase. Miller indices for the cubic phase are given to the left, and those for the tetragonal phase to the right. Also indicated in the figure is the c/a ratio, which is unity for the cubic phase and about 0.9 for the tetragonal phase.

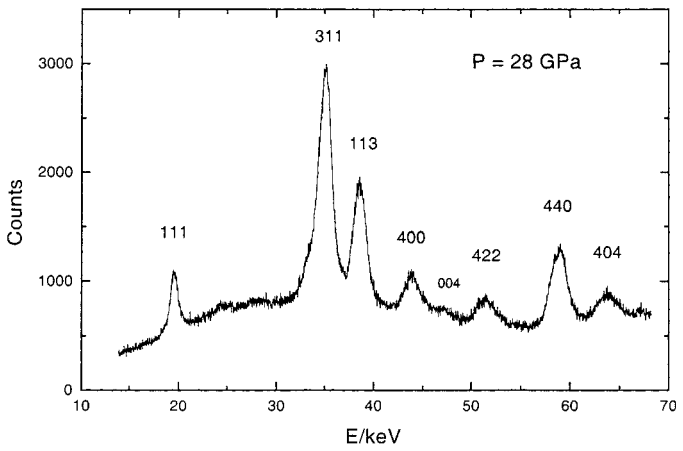

Figure 9. Indexed energy-dispersive diffraction spectrum of tetragonal $CuMn_2O_4$ at 28 GPa. Bragg angle $\theta = 3.92^\circ$, refined lattice constants $a = 8.20(10)$ and $c = 7.65(12)$ Å.

justified by superexchange coupling between the A and B sublattices, and the fact that the local ferromagnetic order of Mn ions on B sites can be disturbed by Cu^{2+} on the same sites.

HP x-ray energy-dispersive diffraction spectra were recorded at room temperature for pressures up to 33 GPa. Figure 8 shows the interplanar spacings, d_{hkl}, of $CuMn_2O_4$ as functions of pressure. New diffraction lines indicate a structural phase transition above 10 GPa. From the appearance of the new lines and the disappearance of the lines of the low-pressure phase, we estimate the transition pressure $P_c = 12.5$ GPa. The diffraction spectra of the high-pressure phase can be indexed according to a tetragonal distortion of the f.c.c. unit cell of the low-pressure phase [38]. The relative intensities of 311 and 113 lines indicate that the c/a ratio of tetragonal unit cell is less than one. In the tetragonal system, the intensity of the 311 line

is about twice the intensity of the 113 line, mainly because of the multiplicity factor. For $c/a < 1$ the 311 line occurs at a lower energy than the 113 line (i.e. $d_{311} > d_{113}$) in accordance with the observed spectrum (figure 9). At 28 GPa we obtain the refined unit-cell parameters $a = 8.20 \pm 0.10$ and $c = 7.65 \pm 0.12$ Å with a goodness of fit $\sum |d_{calc} - d_{obs}| / \sum d_{obs} = 1.4\%$, which is a reasonably good figure for energy-dispersive high-pressure diffraction spectra. It may be mentioned that a fit with $c/a > 1$ results in a too small unit-cell volume. It is found that the c/a ratio is about 0.9 independent of pressure (figure 8). A similar value was previously found for the tetragonal high-pressure phase of $NiMn_2O_4$ [22].

There is a puzzling disappearance of the relatively intense 220 line at the transition. The tetragonal 220/202 doublet is visible in the beginning of the phase transition, in the pressure range 10–14 GPa, as shown in figure 8, but it disappears at higher pressures. On the other hand, the relatively weak 111 reflection is visible throughout the observed pressure range. The reason for this behaviour could be non-hydrostatic conditions or preferred orientations in the sample at high pressure.

The experimental pressure–volume data for the cubic low-pressure phase can be described by the Birch equation of state [39]:

$$P/B_0 = \tfrac{3}{2}(x^{-7} - x^{-5})[1 + \tfrac{3}{4}(B_0' - 4)(x^{-2} - 1)] \tag{4}$$

where $x = a/a_0$, a being the lattice constant at pressure P and a_0 the zero-pressure lattice constant. B_0 is the bulk modulus and B_0' its pressure derivative, both parameters evaluated at zero pressure. The scatter of the data did not allow the use of B_0' as a fitting parameter. Instead, it was assumed that $B_0' = 4.00$, which is a typical value for most solids. The fit of the Birch equation of state to the experimental data points was restricted to $P \leqslant 9$ GPa in order to avoid possible problems with nonhydrostatic conditions at higher pressures.

For the bulk modulus we obtain $B_0 = 198 \pm 6$ GPa where the uncertainty is the standard deviation from the fit. In comparison, we have previously found 206 ± 4 GPa for $NiMn_2O_4$ [22] and 197 ± 5 GPa for $ZnMn_2O_4$ [24]. It may also be mentioned that the bulk modulus for the mineral spinel ($MgAl_2O_4$) is 196 GPa. These results agree well with the hypothesis, suggested by Finger *et al* [40] and recently confirmed theoretically by Pendás *et al* [41], that all oxide spinels should have a bulk modulus about 200 GPa. The oxygen ions are forming a nearly close-packed sublattice, occupying most of the available space. At the same time they are relatively easy to deform and in this way the oxygen ions are determining the overall compressibility of the oxide spinels.

The equation of state—when extrapolated—is seen to describe the pressure–volume behaviour in the entire pressure range, including the tetragonal high-pressure phase (figure 10). Accordingly there is no discontinuity in volume and bulk modulus at the cubic-to-tetragonal phase transition.

Without knowing the HP structure and the cation distribution in detail, some simple model of this phase can be derived from the pressure dependence of the unit cell parameters. The volume contraction and character of the unit cell deformation (figure 11) implies that due to reduced length of the c axis, the A sites are too small to accommodate the Cu^+ ions, therefore the charge exchange of the type Cu_A^+–O–$Mn_B^{4+} \rightarrow Cu_A^{2+}$–O–$Mn_B^{3+}$ takes place. Simultaneously, fast hopping of electron between Mn^{3+} and Mn^{4+} on the B sites may cause formation of the JT active Mn^{3+} ions in a number sufficient for the tetragonal deformation, thus we have

$$Cu_{0.2}^{2+}Mn_{0.8}^{2+}[Cu_{0.8}^{2+}Mn_{1.2}^{3+/4+}]O_4. \tag{5}$$

Another superexchange process can be imagined for the pair Mn_A^{2+}/Mn_B^{4+}, i.e. Mn_A^{2+}–O–$Mn_B^{4+} \rightarrow Mn_A^{3+}$–O–$Mn_B^{3+}$, which leads to the ionic distribution

$$Cu_{0.2}^{2+}Mn_{0.8}^{3+}[Cu_{0.8}^{2+}Mn_{1.2}^{3+}]O_4. \tag{6}$$

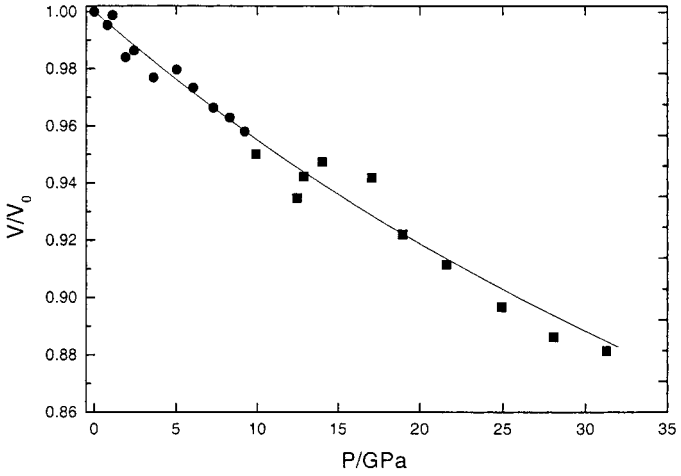

Figure 10. Relative volume of $CuMn_2O_4$ as a function of pressure. The notation is as for figure 8. The full curve is an extrapolation of the Birch equation which was fitted to the experimental data for $P \leqslant 9$ GPa.

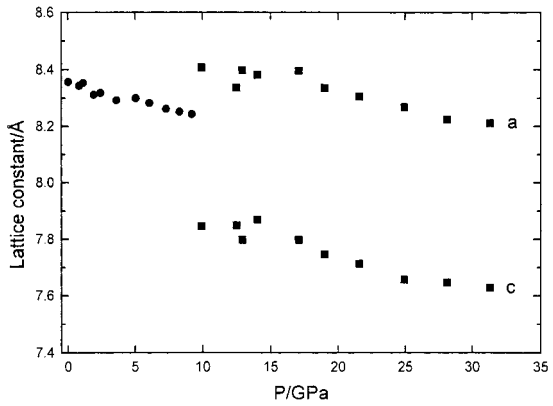

Figure 11. Pressure change of the unit cell parameters.

At ambient conditions Mn^{3+} shows strong site preference for the octahedral coordination, therefore the formula (6) can be accepted with an assumption that at high pressure the ligand field forces the charge exchange Mn_A^{2+}/Mn_B^{3+}.

4. Conclusions

At ambient conditions both the metal ions are JT active at either site, but while at the tetrahedral ones they gain some amount of stabilization energy by compressed configuration, at the octahedral sites the usual distortion is an elongated oxygen octahedron. The pressure-induced changes of the interatomic distances influence the electrostatic interactions between the ligands and metal cations in the crystal fields of octahedral and tetrahedral symmetries. Elongation of the a axis and the concomitant contraction of the c axis above P_c indicates that the MO_6^{2-} units on the B sites are not regular octahedra anymore. The two M–O distances along the c axis are shorter than the four others in the equatorial plane. As it was mentioned in the introduction,

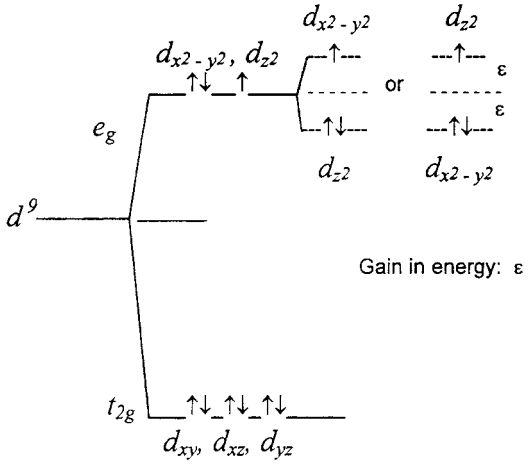

Figure 12. Schematic energy diagram of change of the electronic configuration in the Jahn–Teller Cu^{2+} (d^9) ion on the octahedral site.

the distortion implies that orbitally degenerate configuration of Cu^{2+} and Mn^{3+} are not stable in the ligand field and the ions reduce their energy by changing their electron configuration. A simple model in figure 12 shows the $Cu^{2+}(3d^9)$ ion in a high spin configuration, with five 3d orbitals split by the octahedral ligand field into the lower triplet (t_{2g}^6), filled with six electrons having antiparallel spin arrangement, and the upper doublet e_g^3, with three electrons which can be distributed in two ways (double degeneracy): $(d_{x^2-y^2})^1(d_{z^2})^2$ and $(d_{x^2-y^2})^2(d_{z^2})^1$. The first alternative, with non-filled orbital $(d_{x^2-y^2})^1$ leads to a stronger attraction between Cu and the oxygen ligands in the (xy) plane. As a result, a Cu–O bond elongation in the vertical direction of the octahedron should thus be observed and this type of prolate deformation usually takes place in temperature dependent transitions (e.g. [43, 44]). The effect of HP in our experiment is just opposite; we observe the crystal volume contraction connected mainly with shortening of the c axis. This implies that the single electron is left on the d_{z^2} orbital, and that the central ion forms a flattened octahedron. Similar consideration can be applied to the Mn^{3+} ions ($3d^4$) with the $(t_{2g}^3)e_g^1$ electron distribution. Three electrons in a high spin configuration are located on the lower triplet, while the fourth one can occupy either the $d_{x^2-y^2}$ or d_{z^2} level of the e_g doublet. At the high-pressure conditions, the single electron on e_g goes to the d_{z^2} orbital, contributing together with Cu^{2+} to the tetragonal distortion corresponding to $c/a < 1$. According to theory the differences between the contracted and elongated octahedral configurations are small, compared with the overall JT energy gain by the distortion. It was estimated that for the compressed configuration the JT energy would be about 5% smaller than for the elongated configuration [45, 46].

One cannot exclude the completely inverse spinel with Cu^+ shifted to the B sites and ionic formula $Mn_{0.8}^{2+}[Cu_1^{2+}Mn_{0.4}^{3+}Mn_{0.8}^{4+}]O_4$. Such configuration was considered in $NiMn_2O_4$, where the inversion parameter increased if the unit cell contracted with decreasing temperature or increasing pressure [21, 42]. Although this is compatible with the site preferences and could explain the tetragonal distortion; this ionic distribution seems, however, less justified as it would require a large amount of energy for the Mn/Cu–O bond reconstruction.

It follows that the origin of the observed structural HP transition in $CuMn_2O_4$ is a change in the electronic structure of the copper and manganese ions, which take the values that they had in the parent oxides Cu^{2+} and Mn^{3+}.

Acknowledgments

The authors thank HASYLAB-DESY, Germany, for permission to use the synchrotron-radiation facility and the Danish Natural Sciences Research Council (DANSYNC) for financial support. The work was supported by the IHP Programme 'Access to research infrastructures' of the European Community under contract No. HPRI-CT-1999-00040.

References

[1] Goodenough J B and Loeb A L 1955 *Phys. Rev.* **98** 391
[2] Robbins M and Darcy L 1966 *J. Phys. Chem. Solids* **27** 741
[3] Blasse G 1966 *J. Phys. Chem. Solids* **27** 383
[4] Baltzer P K and Lopatin E 1964 *Proc. Int. Conf. on Magnetism (Nottingham)*
[5] Sinha A P B, Sanjana N R and Biswas A B 1957 *Acta Crystallogr.* **10** 439
[6] Jogalekar P P 1967 *Indian J. Pure Appl. Phys.* **5** 9
[7] O'Keeffe M 1961 *J. Phys. Chem. Solids* **21** 172
[8] Åsbrink S 1965 *Acta Chem. Scand.* **19** 1776 and references therein.
[9] Meenakshisundaram A, Gunasekaran N and Srinivasan V 1982 *Phys. Status Solidi* a **69** K15
[10] Buhl A 1969 *J. Phys. Chem. Solids* **30** 805
[11] Zaslavskii A I and Plakhtii V I 1969 *Sov. Phys.–Solid State* **11** 672
[12] Radhakrishnan N K and Biswas A B 1977 *Phys. Status Solidi* a **44** 45
[13] Miyahara S 1962 *J. Phys. Soc. Japan* **17** (Suppl.) B181
[14] Kulkarni D K and Mande C 1974 *Indian J. Pure Appl. Phys.* **12** 60
[15] Ghare D B, Sinha A B P and Singh L 1968 *J. Mater. Sci.* **3** 389
[16] Miller A 1968 *J. Phys. Chem. Solids* **29** 633
[17] Padalia D B, Krishnan V, Patni M J, Radhakrishnan N K and Gupta S N 1973 *J. Phys. Chem. Solids* **34** 1173
[18] Dreiling M J 1977 *J. Phys. Chem. Solids* **37** 121
[19] Orgel L E 1960 *Introduction to Transition-Metal Chemistry; Ligand-Field Theory* (London: Methuen)
[20] Wells F 1984 *Structural Inorganic Chemistry* 5th edn (Oxford: Clarendon) pp 87–92
Dunitz J D and Orgel L E 1957 *J. Phys. Chem. Solids* **3** 20
[21] Åsbrink S, Waśkowska A, Drozd M and Talik E 1997 *J. Phys. Chem. Solids* **58** 725
[22] Åsbrink S, Waśkowska A, Staun Olsen J and Gerward L 1998 *Phys. Rev.* B **57** 4972
[23] Åsbrink S, Waśkowska A and Talik E 1998 *J. Phys. Chem. Solids* **60** 573
[24] Åsbrink S, Waśkowska A, Staun Olsen J, Gerward L and Talik E 1999 *Phys. Rev.* B **60** 12 651
[25] Sheldrick G M 1993 *SHELXL'93 Program System for Crystal Structure Refinement* Madison, WI, USA
[26] Mao H K, Bell P M, Shaner J W and Steinberg D J 1978 *J. Appl. Phys.* **49** 3276
[27] Yamada A 1996 *J. Solid State Chem.* **122** 160
[28] Brabers V A M and van Setten F M 1983 *J. Phys. D: Appl. Phys.* **16** L169
[29] Hüfner S 1996 *Photoelectron Spectroscopy: Principles and Application* (Berlin: Springer)
[30] Lindberg P A P, Shen Z X, Spices W E and Lindau I 1990 *Surf. Sci.* **11** 1
[31] Ghijsen J, Tjeng L H, Eskes H, Sawatzky G A and Johnson R L 1990 *Phys. Rev.* B **42** 2268
[32] Töpfer J, Feltz A, Gräf D, Hackl B, Raupach L and Weissbrodt P 1992 *Phys. Status Solidi* a **134** 405 and references [22] and [23] therein
[33] Saitoh T, Bocquet A E, Mizokawa T, Namatame H, Fujimori A, Abbate M, Takeda Y and Takano M 1995 *Phys. Rev.* B **51** 13 942
[34] Wertheim G K, Hüfner S and Guggenheim H 1973 *Phys. Rev.* B **7** 556
[35] Fujimori A, Kimizuka N, Akahane T, Chiba T, Kimura S, Minami F, Siratori K, Taniguchi M, Ogawa S and Suga S 1990 *Phys. Rev.* B **42** 2268
[36] Ghijsen J, Tjeng L H, van Elp J, Eskes H, Westerink J, Sawatzky G A and Czyżyk M T 1990 *Phys. Rev.* B **42** 2268
[37] Balzarotti A, De Crescenzi M, Motta N, Patella F and Sgarlatta A 1988 *Phys. Rev.* B **38** 6461
[38] Gerward L, Staun Olsen J and Benedict U 1986 *Physica* B **144** 72
[39] Birch F 1938 *J. Appl. Phys.* **9** 279
[40] Finger L W, Hazen R M and Hofmeister A 1986 *Phys. Chem. Miner.* **13** 215
[41] Pendás A M, Costales A, Blanco M A, Recio J M and Luaña V 2000 *Phys. Rev.* B **62** 13 970
[42] de Vidales M, Rojas R M, Vila E and Garcia-Martinez O 1994 *Mater. Res. Bull.* **29** 1163
[43] Khomsky D J and Sawatzky G A 1997 *Solid State Commun.* **102** 87

[44] Yamaguchi H, Yamada A and Uwe H 1998 *Phys. Rev.* B **58** 8
[45] Grefer J and Reinen D 1973 *Z. Naturf.* a **28** 464
[46] Winkelmann M, Graf H A, Wagner B and Hewat A W 1994 *Z. Kristallogr.* **209** 870